

# Extension of nano-confined DNA: quantitative comparison between experiment and theory

V. Iarko<sup>1</sup>, E. Werner<sup>1</sup>, L. K. Nyberg<sup>2</sup>, V. Müller<sup>2</sup>, J. Fritzsche<sup>3</sup>, T. Ambjörnsson<sup>4</sup>,  
J. P. Beech<sup>5</sup>, J. O. Tegenfeldt<sup>5,6</sup>, K. Mehlig<sup>7</sup>, F. Westerlund<sup>2</sup>, B. Mehlig<sup>1</sup>

<sup>1</sup>*Department of Physics, University of Gothenburg, Sweden*

<sup>2</sup>*Department of Biology and Biological Engineering, Chalmers University of Technology, Sweden*

<sup>3</sup>*Department of Applied Physics, Chalmers University of Technology, Sweden*

<sup>4</sup>*Department of Astronomy and Theoretical Physics, Lund University, Sweden*

<sup>5</sup>*Department of Physics, Division of Solid State Physics, Lund University, Sweden*

<sup>6</sup>*NanoLund, Lund University, Sweden and*

<sup>7</sup>*Department of Public Health and Community Medicine, University of Gothenburg, Sweden*

The extension of DNA confined to nanochannels has been studied intensively and in detail. Yet quantitative comparisons between experiments and model calculations are difficult because most theoretical predictions involve undetermined prefactors, and because the model parameters (contour length, Kuhn length, effective width) are difficult to compute reliably, leading to substantial uncertainties. Here we use a recent asymptotically exact theory for the DNA extension in the ‘extended de Gennes regime’ that allows us to compare experimental results with theory. For this purpose we performed new experiments, measuring the mean DNA extension and its standard deviation while varying the channel geometry, dye intercalation ratio, and ionic buffer strength. The experimental results agree very well with theory at high ionic strengths, indicating that the model parameters are reliable. At low ionic strengths the agreement is less good. We discuss possible reasons. Our approach allows, in principle, to measure the Kuhn length and effective width of a single DNA molecule and more generally of semiflexible polymers in solution.

PACS numbers: 87.15.-v, 36.20.Ey, 87.14.gk

Nano-confined DNA has recently been intensively studied [1–6] as a means of stretching the molecules in order to study local properties (e.g. DNA sequence [7, 8]). A fundamental question is how the physical properties of the DNA and the solution affect the extent to which the molecule is stretched by confinement. Experimentally this question has been investigated in detail, varying the confinement, the length of the DNA molecule, and the properties of the solution (see Ref. [1] for a review).

It is commonly assumed that DNA can be modeled as a semiflexible polymer with hard-core repulsive interactions [9–15]. Measurements [16–19] and theoretical considerations [9, 16] indicate that a worm-like chain model may be a good approximation. A recent study [3] compares experimental results for the extension of confined  $\lambda$ -DNA to results of computer simulations of a self-avoiding discrete worm-like chain model, indicating that it may describe the experimental results well.

Yet quantitative comparison between experiments and theoretical model calculations has remained difficult for at least two reasons. First the model parameters (contour length, Kuhn length  $\ell_K$ , and effective width  $w_{\text{eff}}$  of the semiflexible polymer) are difficult to determine reliably: there is substantial uncertainty regarding the physical properties of DNA. Second, the model is hard to analyse theoretically. But a recent asymptotically exact theory [20, 21] for the extension of a confined self-avoiding semiflexible polymer in the so-called ‘extended de Gennes regime’ [11, 13, 22] overcomes the second difficulty: it makes precise predictions for the prefactors

and exponents defining scaling laws as a function of the physical parameters, Eqs. (2) below. This opens the possibility to experimentally determine  $\ell_K$  and  $w_{\text{eff}}$  by measurements of confined DNA. In this article we report on experimental results mapping out how the extension of confined DNA in the extended de Gennes regime depends on channel geometry, ionic strength of the solution, and upon the amount of dye bound to the molecule.

At high ionic strengths we find very good agreement between experiment and theory using approximations for  $\ell_K$  and  $w_{\text{eff}}$  that are commonly employed [23–26], and taking into account how the contour length depends on the amount of dye molecules bound to the DNA. The comparison between experiment and theory is so precise that it enables us to detect subtle alignment effects [27] at the border of the extended de Gennes regime. At low ionic strengths the agreement is not as good. This may indicate that theoretical estimates of  $\ell_K$  and  $w_{\text{eff}}$  must be improved. We expect it is possible to experimentally precisely determine  $\ell_K$  and  $w_{\text{eff}}$  by extending the approach described in this article.

*Extended de Gennes regime.* Consider a semiflexible polymer of contour length  $L$ , Kuhn length  $\ell_K$  [9] and excluded volume  $v$  per Kuhn length segment. The excluded volume is often written in terms of an effective width  $w_{\text{eff}}$ , defined by the relation  $v \equiv (\pi/2)\ell_K^2 w_{\text{eff}}$ . This expression for the excluded volume is based on Onsager’s result [28] for the excluded volume of a cylinder of length  $\ell_K$  and diameter  $w_{\text{eff}}$ , which in the limit  $\ell_K \gg w_{\text{eff}}$  reduces to the expression above. We phrase our results in terms of

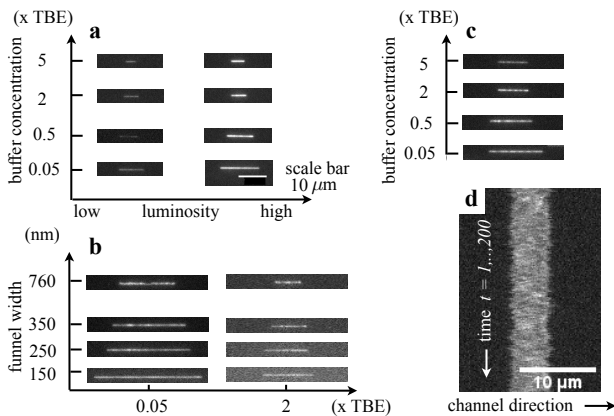


FIG. 1: **a** Experiment 1.  $\lambda$ -DNA in a  $150 \text{ nm} \times 108 \text{ nm}$  channel, different buffer concentrations, and different luminosities corresponding to different dye loadings. Shown are representative video frames (scale bar applies to panels **b**, **c** as well). **b** Experiment 2. T4-DNA in a nanofunnel in  $0.05\times$  and  $2\times$ TBE solution, varying funnel width  $D_W$  at constant  $D_H = 120 \text{ nm}$ . **c** Experiment 3. T4-DNA in a  $302 \text{ nm} \times 300 \text{ nm}$  channel, different buffer concentrations. **d** Time trace of the fluorescence intensity for  $\lambda$ -DNA in a  $108 \text{ nm} \times 150 \text{ nm}$  channel in  $5\times$ TBE solution, center-of-mass motion subtracted.

the effective width  $w_{\text{eff}}$ . This is customary but we stress that, strictly speaking, it is the excluded volume that determines the statistics of the polymer, and that even for DNA models with only hard-core repulsion between rod-like segments, the effective width does not equal the actual width of the rods, except in the limit  $\ell_K \gg w_{\text{eff}}$ . This is important to consider when evaluating the results of simulations.

The polymer is confined to a channel with cross section  $D_W \times D_H$ . The polymer exhibits different confinement regimes distinguished by different laws for the polymer extension in the channel direction [21]. The extended de Gennes regime is defined by the conditions [21]

$$\ell_K \ll D_H \ll \ell_K^2/w_{\text{eff}} \quad \text{and} \quad D_W^2 \ll D_H \ell_K^2/w_{\text{eff}}, \quad (1)$$

where we assume that  $D_W \geq D_H$ . For a square channel the corresponding conditions were previously derived and discussed in Refs. [10, 11, 13, 20, 22]. In regime (1) exact expressions for the mean  $\mu$  and the variance  $\sigma^2$  of the extension in the channel direction are known [20, 21], provided that the contour length is long enough [20]:

$$\mu/L = 0.9338(84) [\ell_K w_{\text{eff}} / (D_W D_H)]^{1/3}, \quad (2a)$$

$$\sigma / (L \ell_K)^{1/2} = 0.364(17). \quad (2b)$$

The errors quoted for the coefficients reflect strict bounds [20] derived from the exact results of Ref. [29]. Provided  $L$  is known Eqs. (2) allow to infer  $\ell_K$  and  $w_{\text{eff}}$  from measurements of nanoconfined DNA molecules.

*Calculation of parameters.* We now discuss how the parameters  $L$ ,  $\ell_K$  and  $w_{\text{eff}}$  are commonly estimated for

	$0.05\times$ TBE	$0.5\times$ TBE	$2\times$ TBE	$5\times$ TBE
$I_s$ [mM]	3.81	24.9	78.4	178.0
$\ell_K$ [nm]	154.4	116.5	105.9	101.2
$w_{\text{eff}}$ [nm]	26	10	6.2	4.6

TABLE I: Numerical values for the ionic buffer strength  $I_s$ , the Kuhn length  $\ell_K$ , and the effective width  $w_{\text{eff}}$  (see text).

DNA, and what the main uncertainties are. We first discuss bare DNA, before considering the effect of staining with fluorescent dye (YOYO-1).

The contour length of bare DNA is  $0.34 \text{ nm}$  per base pair, with an uncertainty of about  $0.01 \text{ nm}$ , or 3% [30].

DNA is commonly modeled as a worm-like chain, for which the Kuhn length is twice the persistence length,  $\ell_K = 2\ell_P$  [9]. The persistence length has been measured by a number of different techniques [16, 17, 19, 31] yielding  $\ell_P \approx 45\text{--}50 \text{ nm}$  at high ionic strength ( $I_s \gtrsim 10 \text{ mM}$ ), and increasing at lower  $I_s$ . Following Refs. [3, 25, 26, 32] we use the empirical formula suggested in Ref. [23]  $\ell_P \approx 46 \text{ nm} + 1.92 I_s^{-1/2} \text{ M}^{1/2} \text{ nm}$ . While this dependence of  $\ell_P$  upon  $I_s$  has a theoretical basis, the prefactors are known only from an empirical fit with an uncertainty of about 10% (Fig. 3 in Ref. [23]). The resulting values of  $\ell_K$  are given in Table I, the calculation of  $I_s$  is described in the Supplemental Material [33].

Stigter [24] computed the excluded volume between two long, strongly charged cylinders in NaCl solution, and applied this calculation to DNA to obtain an estimate of  $w_{\text{eff}}$ . Linear interpolation on a doubly logarithmic scale of the effective widths given in Table 1 of Ref. [24] yields the values tabulated in Table I. There are many sources of uncertainty when applying this theory to our system. Stigter's calculation [24] for  $w_{\text{eff}}$  assumes that the Kuhn length segments can be approximated by infinitely long cylinders with an intrinsic width of  $1.2 \text{ nm}$ , and that the effective line charge of DNA is given by  $0.73e^-$  per phosphate group. The approximation of infinite cylinders is problematic when the Kuhn length and the effective width are of the same order, i.e. for low ionic strengths. According to Stigter, the value  $1.2 \text{ nm}$  has an uncertainty of about 20%, leading to an uncertainty for the effective width of 5-10% [34], with a larger effect at large ionic strengths. The effective line charge estimate is based on measurements in NaCl-solutions, which do not generalise to other ions [35].

The DNA contour length is expected to increase in proportion to the amount of dye bound. We assume that dye intercalation extends the bare contour length of the DNA molecule by  $0.44 \text{ nm}$  per dye molecule [3]. Estimates of this number range from about  $0.4 \text{ nm}$  to  $0.5 \text{ nm}$ , with large uncertainties in the individual estimates [36, 37], the uncertainty is at least 10%. At a dye loading of 1 molecule per 10 base pairs, this corre-

sponds to an uncertainty in the contour length of  $\approx 2\%$ . There is no consensus regarding how intercalating dye molecules affect the parameters  $\ell_K$  and  $w_{\text{eff}}$ . Ref. [38] finds that the Kuhn length decreases with increasing dye load, whereas Ref. [37] finds no dependence. Since the dye molecules are positively charged, the effective width might decrease with dye load, but the magnitude of this effect is not known. Lacking a better estimate, it is commonly assumed that YOYO-binding does not affect these parameters [3, 26, 39]. In summary, while the contour length of DNA is known to a rather high accuracy, there is substantial uncertainty regarding the parameters  $\ell_K$  and  $w_{\text{eff}}$ .

*Experimental method.* The experimental data are obtained measuring the extension of single DNA molecules in nanochannels under different conditions (Fig. 1a to c). We use linear  $\lambda$ - and T4GT7-DNA (T4-DNA for short) with definite contour lengths of 48502 and 165647 base pairs, respectively (this ensures that  $L$  is large enough in our experiments, it exceeds  $(D_W^2 D_H^2 \ell_K / w_{\text{eff}}^2)^{1/3}$  by an order of magnitude [21]). The molecules are stained with YOYO dye and suspended inside a channel in a TBE (Tris-Borate-EDTA) buffer.

The first experiment is a re-analysis of data presented in Ref. [32]. In this experiment (Fig. 1a),  $\lambda$ -DNA is inserted into a nanochannel of height  $D_H = 150$  nm and width  $D_W = 108$  nm. We discuss the uncertainty in the channel dimensions in the Supplemental Material [33]. DNA extensions are measured at different buffer conditions ( $0.05\times$ ,  $0.5\times$ ,  $2\times$  and  $5\times$ TBE), and at different dye loads. To estimate the dye load of a molecule we assume that it is proportional to the luminosity, and that the largest observed luminosity corresponds to full intercalation (one dye molecule per four base pairs). In this way we obtain an estimate for the amount of dye bound to the molecule by linear interpolation.

In experiment 2 (Fig. 1b), T4-DNA is inserted into a nanofunnel, with fixed height  $D_H = 120$  nm and gradually changing width from  $D_W = 92$  nm to  $D_W = 815$  nm over a length of  $500 \mu\text{m}$ . These experiments are at two different buffer concentrations ( $0.05\times$  and  $2\times$ TBE).

In experiment 3 (Fig. 1c), T4-DNA is inserted into a channel with  $D_W = 302$  nm,  $D_H = 300$  nm. The buffer concentration is varied ( $0.05\times$ ,  $0.5\times$ ,  $2\times$ , and  $5\times$ TBE). In experiments 2 and 3, the average dye load at  $0.05\times$ TBE is approximately 1 dye molecule per 10 base pairs. Assuming that the dye load is proportional to luminosity we estimate the dye load in experiment 2 at  $2\times$ TBE to 1 dye molecule per 45 base pairs, and 1 per 12, 16, 28 base pairs at  $0.5\times$ ,  $2\times$ , and  $5\times$ TBE in experiment 3.

For each molecule 200 frames are recorded. Fig. 1d shows an example of a fluorescence-intensity trace (‘kymograph’) obtained in this way. Each row in the kymograph shows the fluorescence intensity in a given frame averaged over the channel cross section. Bright regions

correspond to high intensity indicating where the DNA molecule is located. The extension of the molecule along the channel is simply the width of the bright region.

For a given set of parameters we estimate the mean and standard deviation of the extension by a linear mixed model that takes into account the fact that the measured extensions are correlated in time. Details concerning the experimental method and the data analysis are given in the Supplemental Material [33].

*Results.* Our results are shown in Fig. 2. We plot two theoretical curves. The solid curve uses the actual channel size  $D_H \times D_W$ . The dashed curve compensates for the repulsive interaction with the negatively charged walls [1], by using an ‘effective channel size’  $(D_H - \delta) \times (D_W - \delta)$ . We take  $\delta = w_{\text{eff}}$ , but it is not known how accurate this estimate is. Since the standard deviation is independent of channel size in the extended de Gennes regime, the compensation does not affect this comparison.

The results of experiment 1 are shown in panels **a** and **b**. At low relative luminosity (small dye-to-basepair ratio) the average extension is well described by Eq. (2a). For the standard deviation there are larger differences between experiment and Eq. (2b). Possible reasons are discussed below.

We turn now to the effect of increasing the dye-to-basepair ratio of the DNA. The theoretical lines are calculated under the assumption that each dye molecule increases the contour length by 0.44 nm but leaves the Kuhn length and the effective width unchanged. This yields estimates of the mean and standard deviation that overestimate the observables at high ionic strengths and high dye loads. A simple explanation would be that the persistence length decreases slightly with increasing dye load, in agreement with Ref. [38] though not with Ref. [37]. Note that since experiments 2 and 3 were performed at low dye-to-basepair ratios, such a decrease would not significantly influence the interpretations of these experiments.

The results of experiment 2 are shown in panels **c**, **d**. Again, the experimental results are in qualitative agreement with the theoretical predictions. We see that the average extension agrees well with the theoretical prediction. However, the model predictions underestimate the standard deviation for the larger ionic strength, and for the largest channel at the lower ionic strength.

It is important to note that for experiment 2 we do not expect perfect agreement with Eqs. (2), since the condition  $D_H \gg \ell_K$  is not satisfied, or only weakly satisfied. However, as long as  $D_W \gg \ell_K$ , the violation of the condition for  $D_H$  only affects the prefactors but not the power of  $D_W$  in Eqs. (2). This follows from the fact that a mapping to a one-dimensional model is possible also when  $D_H \approx \ell_K$  [21]. In accordance with this prediction, the data points satisfying  $D_W \gg \ell_K$  in panel **c** obey the scaling  $\mu \propto D_W^{-1/3}$  of (Eq. 2a). Similarly the data points at  $2\times$ TBE which satisfy  $D_W \gg \ell_K$  show a variance that

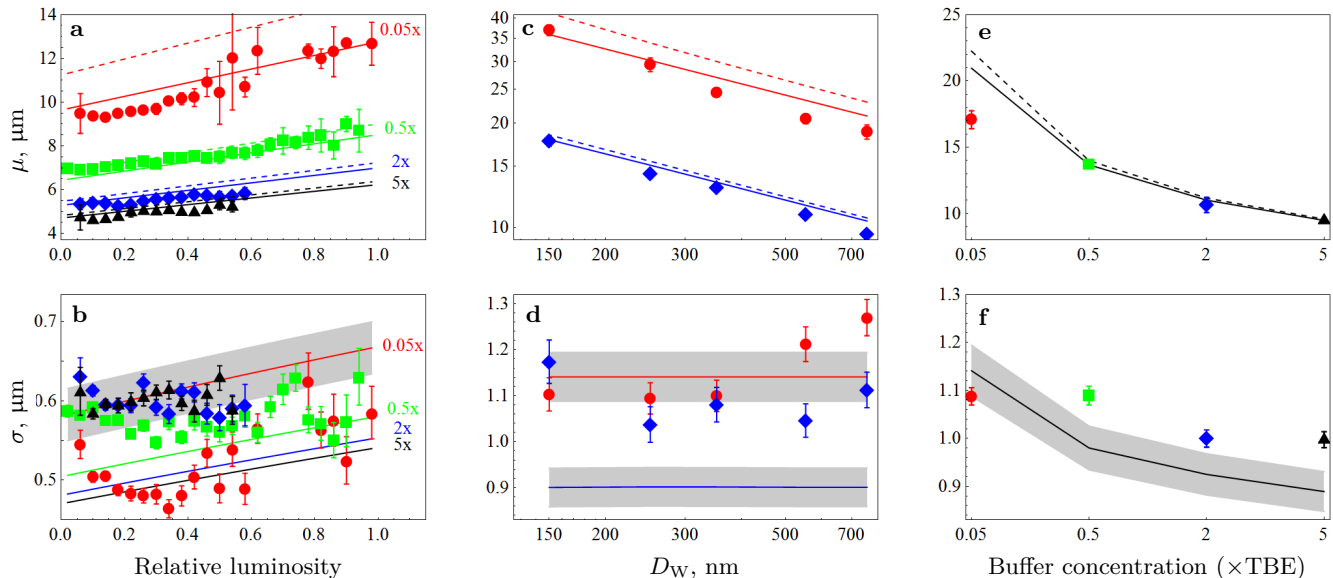


FIG. 2: Experimental results for  $0.05\times\text{TBE}$  (red  $\circ$ ),  $0.5\times\text{TBE}$  (green  $\square$ ),  $2\times\text{TBE}$  (blue  $\diamond$ ), and  $5\times\text{TBE}$  (black  $\triangle$ ) **a**, **b** Experiment 1. Mean and standard deviation of the extension of  $\lambda$ -DNA in a narrow nanochannel, as a function of relative luminosity. Theory [Eq. (2)], solid lines. The rigorous bounds on the prefactor in Eq. (2b) are indicated as a shaded region for  $0.05\times\text{TBE}$ , they are of the same order for the other cases. The corresponding uncertainty for the extension is much smaller and not shown. The dashed line shows theory corrected for wall repulsion (see text). **c**, **d** Experiment 2. Same, but for T4-DNA in a nanofunnel with varying width  $D_W$ . Note that panel **c** is a log-log plot. **e**, **f** Experiment 3. Same, but for T4-DNA in a wider square nanochannel, as a function of buffer concentration ( $x\times\text{TBE}$ ). Error bars correspond to 95% confidence intervals from the statistical analysis, the experimental uncertainty is not taken into account.

is approximately independent of  $D_W$ , in agreement with Eq. 2b, Fig. 2d. For the two rightmost data points at  $0.05\times\text{TBE}$ , the condition  $D_W^2 \ll D_H \ell_K^2 / w_{\text{eff}}$  is violated. At this point the variance is expected to start increasing as  $D_W$  increases further [21], in perfect agreement with what is observed.

For square channels simulations [11, 15, 22] show that the mean extension increases more rapidly with decreasing  $D = D_H = D_W$  than Eq. (2a) predicts, when  $D \approx \ell_K$ . The reason is that there is a tendency for the DNA molecule to align with the wall, and that the presence of the walls makes it more difficult for the molecule to change direction in the channel, forming a ‘hairpin’ [15, 27]. This can explain why the average extension appears to increase slightly faster with decreasing width than Eq. (2a) predicts, for the leftmost points in panel **c**. Such a trend has also been observed in previous measurements in rectangular channels [27, 40].

Now consider the standard deviation. The alignment and correlation effects mentioned above cause  $\sigma$  to be overestimated [27]. But when  $\mu$  approaches the maximal extension  $L$  then fluctuations are suppressed [15]. These two effects could explain why, in experiments 1 and 2,  $\sigma$  is larger than predicted by theory at high ionic strengths but smaller for low ionic strengths and small channel sizes. It must also be noted that the standard deviation is difficult to estimate precisely, as it is not very much larger than the pixel size in the image (159 nm),

and may depend on the assumptions entering into the statistical analysis (see Supplemental Material [33]). An additional source of uncertainty specific to experiment 2 is that  $D_W$  changes over the span of the molecule. For the most extended condition ( $\mu = 37 \mu\text{m}$ ), the channel width at either end of the molecule differs by approximately 25 nm from the stated width, measured at the center of the molecule.

The results of experiment 3 are shown in panels **e**, **f**. Here Eq. (1) is well satisfied. Simulations indicate [15, 22] that the alignment effects discussed above have little influence on  $\mu$ , in square channels with  $D \approx 3\ell_K$ . Equally sensitive simulation results for  $\sigma$  have not been published, but simulations of the alignment effect [15, 27] indicate that Eq. (2b) underestimates  $\sigma$  by approximately 10%. We find that for the three largest ionic strengths, measurements are in excellent agreement with theory. The mean extension (panel **f**) agrees very well with the theoretical prediction of Eq. (2a), and Eq.(2b) underestimates the standard deviation (panel **f**) by about 10%, just as the measurements of alignment effects would suggest.

Intriguingly, the relation between measurements and predictions is different at  $0.05\times\text{TBE}$  than at high ionic strengths. Both mean and standard deviation are smaller than expected. This is particularly surprising considering that alignment effects should be even stronger at low ionic strength (where  $\ell_K$  is larger). The discrepancy might indicate that the standard model does not describe

the physical parameters well at such low ionic strengths, possibly because the high relative concentration of BME significantly changes the buffer conditions, lowering the pH from  $\approx 8.5$  to  $\approx 7.5$ . But we note that it may be hard to ensure uniform dye coverage under these conditions [32]. Also, BME is consumed as the experiment proceeds. This may change the ionic strength at small buffer concentrations, an effect our calculations do not include.

*Conclusions.* We have compared measurements of the extension of confined DNA to asymptotically exact predictions. First, we find very good agreement between experiments and theoretical predictions at high ionic strengths. A possible cause for deviations at low ionic strengths is that common estimates for  $w_{\text{eff}}$  and  $\ell_K$  of stained DNA are too imprecise. Second, by measuring longer time series and more molecules in wider channels we expect to be able to precisely determine how  $\ell_K$  and  $w_{\text{eff}}$  depend on the ionic strength of the solution. It may even be possible to determine  $\ell_K$  and  $w_{\text{eff}}$  for single molecules. We note that  $w_{\text{eff}}$  is an effective parameter defined in terms of the excluded volume per Kuhn length, even for rigid rods  $w_{\text{eff}}$  is identical to the actual width only when  $\ell_K \gg w_{\text{eff}}$ . Finally the approach described here could be used to investigate DNA-wall interactions, a question about which little is known, and that is hard to describe theoretically.

*Acknowledgements.* This work was made possible through support from the Swedish Research Council (BM), the Göran Gustafsson Foundation for Research in Natural Sciences and Medicine (BM), Chalmers Area of Advance (FW). We thank Charleston Noble and Erik Lagerstedt for helpful discussions.

After submission of this manuscript a paper [41] appeared online, which also compares experimental measurements on channel-confined DNA to the theoretical predictions of Ref. [20].

- 
- [1] W. Reisner, J. N. Pedersen, and R. H. Austin, *Rep. Prog. Phys.* **75**, 106601 (2012).
- [2] J. J. Jones, J. R. C. van der Maarel, and P. S. Doyle, *Phys. Rev. Lett.* **110**, 068101 (2013).
- [3] D. Gupta, J. Sheats, A. Muralidhar, J. J. Miller, D. E. Huang, S. Mahshid, K. D. Dorfman, and W. Reisner, *J. Chem. Phys.* **140**, 214901 (2014).
- [4] A. Khorshid, P. Zimny, D. Tétreault-La Roche, G. Massarelli, T. Sakaue, and W. Reisner, *Phys. Rev. Lett.* **113**, 268104 (2014).
- [5] M. Alizadehheidari, E. Werner, C. Noble, M. Reiter-Schad, L. K. Nyberg, J. Fritzsche, B. Mehlig, J. O. Tegenfeldt, T. Ambjörnsson, F. Persson, et al., *Macromolecules* **48**, 871 (2015).
- [6] W. F. Reinhart, J. G. Reifengerger, D. Gupta, A. Muralidhar, J. Sheats, H. Cao, and K. D. Dorfman, *J. Chem. Phys.* **142**, 064902 (2015).
- [7] E. Lam, A. Hastie, C. Lin, D. Ehrlich, S. K. Das, M. D. Austin, P. Deshpande, H. Cao, N. Nagarajan, M. Xiao, et al., *Nature Biotechnol.* **30**, 771 (2012).
- [8] A. N. Nilsson, G. Emilsson, L. K. Nyberg, C. Noble, L. S. Stadler, J. Fritzsche, E. R. B. Moore, J. O. Tegenfeldt, T. Ambjörnsson, and F. Westerlund, *Nucl. Acids Res.* **86**, e188 (2014).
- [9] A. Y. Grosberg and A. R. Khokhlov, *Statistical Physics of Macromolecules* (AIP press, 1994).
- [10] T. Odijk, *Phys. Rev. E* **77**, 060901 (2008).
- [11] Y. Wang, D. R. Tree, and K. D. Dorfman, *Macromolecules* **44**, 6594 (2011).
- [12] D. R. Tree, Y. Wang, and K. D. Dorfman, *Phys. Rev. Lett.* **108**, 228105 (2012).
- [13] L. Dai and P. S. Doyle, *Macromolecules* **46**, 6336 (2013).
- [14] A. Muralidhar, D. R. Tree, Y. Wang, and K. D. Dorfman, *J. Chem. Phys.* **140**, 084905 (2014).
- [15] A. Muralidhar, D. R. Tree, and K. D. Dorfman, *Macromolecules* **47**, 8446 (2014).
- [16] P. J. Hagerman, *Annual Review of Biophysics and Biophysical Chemistry* **17**, 265 (1988).
- [17] S. B. Smith, L. Finzi, and C. Bustamante, *Science* **258**, 1122 (1992).
- [18] M. D. Wang, H. Yin, R. Landick, J. Gelles, and S. M. Block, *Biophysical Journal* **72**, 1335 (1997).
- [19] C. Bouchiat, M. D. Wang, J.-F. Allemand, T. Strick, S. M. Block, and V. Croquette, *Biophysical Journal* **76**, 409 (1999).
- [20] E. Werner and B. Mehlig, *Phys. Rev. E* **90**, 062602 (2014).
- [21] E. Werner and B. Mehlig, *Phys. Rev. E* **91**, 050601(R) (2015).
- [22] L. Dai, J. van der Maarel, and P. S. Doyle, *Macromolecules* **47**, 2445 (2014).
- [23] A. V. Dobrynin, *Macromolecules* **39**, 9519 (2006).
- [24] D. Stigter, *Cell Biophys.* **11**, 139 (1987).
- [25] W. Reisner, J. P. Beech, N. B. Larsen, H. Flyvbjerg, A. Kristensen, and J. O. Tegenfeldt, *Phys. Rev. Lett.* **99**, 058302 (2007).
- [26] C.-C. Hsieh, A. Balducci, and P. S. Doyle, *Nano Letters* **8**, 1683 (2008).
- [27] E. Werner, F. Persson, F. Westerlund, J. O. Tegenfeldt, and B. Mehlig, *Phys. Rev. E* **86**, 041802 (2012).
- [28] L. Onsager, *Ann. N. Y. Acad. Sci.* **51**, 627 (1949).
- [29] R. van der Hofstad, F. den Hollander, and W. König, *Probability Theory and Related Fields* **125**, 483 (2003).
- [30] R. R. Sinden, *DNA Structure and Function* (Elsevier, 2012).
- [31] C. G. Baumann, S. B. Smith, V. A. Bloomfield, and C. Bustamante, *Proc. Natl. Acad. Sci.* **94**, 6185 (1997).
- [32] L. Nyberg, F. Persson, B. Åkerman, and F. Westerlund, *Nucleic Acids Research* **41**, e184 (2013).
- [33] See Supplemental Material at [URL will be inserted by publisher] for brief discussions of the statistical analysis, and of the details of the experimental procedure.
- [34] D. Stigter, *Biopolymers* **16**, 1435 (1977).
- [35] J. A. Schellman and D. Stigter, *Biopolymers* **16**, 1415 (1977).
- [36] F. Johansen and J. P. Jacobsen, *Journal of Biomolecular Structure and Dynamics* **16**, 205 (1998).
- [37] K. Günther, M. Mertig, and R. Seidel, *Nucleic Acids Research* **38**, 6526 (2010).
- [38] C. U. Murade, V. Subramaniam, C. Otto, and M. L. Bunnink, *Nucleic Acids Research* **38**, 3423 (2010).

- [39] W. Reisner, K. Morton, R. Riehn, Y. Wang, Z. Yu, M. Rosen, J. Sturm, S. Chou, E. Frey, and R. Austin, *Phys. Rev. Lett.* **94**, 196101 (2005).
- [40] F. Persson, P. Utko, W. Reisner, N. B. Larsen, and A. Kristensen, *Nano Lett.* **9**, 1382 (2009).
- [41] D. Gupta, J. J. Miller, A. Muralidhar, S. Mahshid, W. Reisner, and K. D. Dorfman, *ACS Macro Letters* **4**, 759 (2015).

# Supplemental material for Extension of nano-confined DNA: quantitative comparison between experiment and theory

V. Iarko<sup>1</sup>, E. Werner<sup>1</sup>, L. K. Nyberg<sup>2</sup>, V. Müller<sup>2</sup>, J. Fritzsche<sup>3</sup>, T. Ambjörnsson<sup>4</sup>,  
J. P. Beech<sup>5</sup>, J. O. Tegenfeldt<sup>5,6</sup>, K. Mehlig<sup>7</sup>, F. Westerlund<sup>2</sup>, B. Mehlig<sup>1</sup>

<sup>1</sup>*Department of Physics, University of Gothenburg, Sweden*

<sup>2</sup>*Department of Biology and Biological Engineering, Chalmers University of Technology, Sweden*

<sup>3</sup>*Department of Applied Physics, Chalmers University of Technology, Sweden*

<sup>4</sup>*Department of Astronomy and Theoretical Physics, Lund University, Sweden*

<sup>5</sup>*Department of Physics, Division of Solid State Physics, Lund University, Sweden*

<sup>6</sup>*NanoLund, Lund University, Sweden and*

<sup>7</sup>*Department of Public Health and Community Medicine, University of Gothenburg, Sweden*

## EXPERIMENTAL PROCEDURE

*Channel manufacture.* The channels were manufactured as described in Ref. [S1]. The nanochannels used in experiment 1 have a depth of  $D_H = 150$  nm. The channel cross-section is not perfectly rectangular, but rather trapezoidal, with a width at the top (bottom) of the channel of 130 nm (87 nm). We assume that these channels can be approximated by rectangular channels with a width  $D_W = 108$  nm, which is the arithmetic mean of the measurements at the top and bottom of the channel. The funnels used in experiment 2 have a depth of approximately  $D_H = 120$  nm, and  $D_W$  increases from 92 nm (top: 111 nm, bottom: 73 nm) at the narrow end to 815 nm (top: 830 nm, bottom: 800 nm) at the wide end – over a length of 500  $\mu\text{m}$ . Finally, the channels used in experiment 3 have a depth  $D_H = 300$  nm, and a width  $D_W = 302$  nm (top: 330 nm, bottom: 275 nm). The dimensions are measured before the channel is closed by the lid. Since the bonding process changes the depth of the channel, our values for the depth of the channels have a relatively large uncertainty of about 10 nm.

*Buffer preparation.* The buffers were obtained by diluting 10 $\times$ TBE tablets from Medicago to the desired concentration. 1 $\times$ TBE contains 0.089 M Tris, 0.089 M Borate and 0.0020 M EDTA. Right before the experiments, 3% BME (3  $\mu\text{L}$  of BME to 97  $\mu\text{L}$  of sample solution) was added to prevent photo-nicking of the DNA. In addition to this the micro- and nanochannels in the chip were flushed with the right buffer concentration, containing 3% BME as well, to keep the same environment in the chip as in the sample solution.

*Dye intercalation.* Since intercalation of YOYO-dye molecules extends the contour length of the DNA it is important to estimate the dye load as accurately as possible. In experiment 1, the dye load was not equilibrated between molecules, resulting in heterogeneous staining [S2]. In experiments 2 and 3 the aim was instead to achieve homogeneous staining. To this end we first mixed the sample in high ionic strength (5 $\times$ TBE), let it rest for at least 20 min, and then diluted to the desired ionic

strength [S2].

*DNA insertion.* The nanofluidic chips consist of four loading wells connected two and two by microchannels. The microchannels are in turn connected by many nanochannels. Sample solution was inserted into one of the loading wells. Then the DNA was carried to the nanochannels by pressure-driven flow (N<sub>2</sub> gas for T4 experiments and air for lambda experiments). The DNA was forced into the nanochannels by applying pressure over two wells that are connected by a microchannel. Once inserted in the channel, the pressure was switched off. Before imaging the DNA was allowed to relax for about 30 seconds to reach its equilibrium extension.

*Video recording.* Videos were recorded using a Photometrics Evolve<sup>TM</sup> EMCCD camera. The image pixel size is 159.2 nm. For all measurements, the exposure time was 100 ms per photograph, but the delay between frames differed between experiments. For experiment 1, the delay between frames was 84 ms, yielding a frame-rate of 184 ms/frame. For experiments 2-3 with T4-DNA, the correlation time is significantly longer, so to minimise problems with photo bleaching and nicking, the frame-rate was decreased. For experiment 2, the frame-rate was 0.5 s/frame for the measurements at 0.05 $\times$  TBE, and 2 s/frame for the ones at 2 $\times$  TBE. For experiment 3, the frame-rate was 1 s/frame for all measurements.

*Number of molecules.* In experiment 1, 2388 molecules were analysed in total. Since the relative intensities are distributed unevenly, so are the number of molecules in each bin. This leads to very different error estimates for different bins in the estimation of the mean and standard deviation. We excluded bins with 2 molecules or less from the analysis. Further 3 molecules were excluded because the extension could not be successfully extracted from all frames. In experiment 2, 9-10 molecules were analysed per data point under 0.05 $\times$ TBE, and 7 molecules under 2 $\times$ TBE. In experiment 3, 30 to 35 molecules were analysed per measured data point. One outlier at 0.5 $\times$  TBE was removed, as its extension changed abruptly halfway through the data series.

## DATA ANALYSIS

*Extraction of DNA extension from kymographs.* Consider a raw kymograph of the form provided in the main text (Fig. 1d). Dark regions in this image correspond to background, the bright regions correspond to fluorescence from DNA. The fluorescence intensities measured for both regions are subject to noise. This makes it difficult to reliably identify the end points of the bright regions in an automated fashion. In previous studies this was achieved by fitting the difference of two sigmoidal functions [S3] to each time frame. This method was used for analysing experiment 1 [S2]. In experiments 2-3 we used a computationally faster method that yields very similar results for the mean, and agrees to within about 5% for the standard deviation of the extension. The new method for detecting end positions relies on the assumption that the fluorescence intensities from DNA and from the background assume consistent and easily differentiated values, and proceeds as follows. First, each frame in the raw kymograph is smoothed using a moving average (we use an averaging window that is five pixels wide). Second, each frame is then segmented into binary low- and high-intensity regions using Otsu’s method [S4, S5]. Third, we even out gaps between high-intensity regions that are equal to or shorter than five pixels. Fourth, the largest connected high-intensity component is found, and its edges are identified. The distance between these edges is the extension of the DNA molecule.

*Statistical analysis.* The experimental data consist of repeated measurements of the extension of individual DNA molecules at given values of parameters and are modeled using a random-coefficient model, a variation of a linear-regression model adapted to correlated data [S6]. Let  $y_{ij}$  denote the extension of molecule  $i$  ( $i = 1, \dots, n$ ) at time  $t_j$  ( $j = 1, \dots, 200$ ). The extension is modeled as a linear function of time as  $y_{ij} = \mu + \beta t_j + u_i + e_{ij}$ , where  $\mu$  and  $\beta$  denote the overall mean value and slope. To account for the within-molecule correlation of data points the error term is split into two uncorrelated components, a molecule-specific correction to the mean,  $u_i$ , and an error term  $e_{ij}$  that measures the deviation of a data point from the molecule-specific regression line,  $\mu + \beta t_j + u_i$ . Both  $u_i$  and  $e_{ij}$  are assumed to be independently normally distributed with mean zero and variance  $r^2$  and  $\sigma^2$ , respectively. The model describes the mean extension of molecules at a particular set of external parameters and the linear time dependence allows to include small unmeasured changes of external conditions, for instance drift into wider or narrower channel regions, or change of buffer concentration. The random intercept adjusts for the initial conditions at the start of measurement of each time series. A random intercept model is adequate as each set of molecules can be viewed as a random sample representative for all molecules at this particular set

of external parameters. On average, the covariance of two arbitrary data points within molecules is equal to the variance of intercepts between molecules. The ratio of variances,  $r^2/(r^2 + \sigma^2)$  is both a measure for the proportion of variation that is explained by differences between molecules, and the correlation of data points within a typical time series. By isolating the molecule-specific random variation due to unknown fluctuations of external parameters we are able to obtain an improved value for the residual variance of the extension ( $\sigma^2$ ) that can be compared with the theory. Although the time trend was weak in most cases, we evaluated the mean value  $\mu$  at  $t = 100$ , i.e. we replaced  $t_j$  with  $(t_j - 100)$  in the above model. Results are given in terms of point estimates together with a 95% confidence interval (95% CI). The statistical analyses were performed by using SAS (version 9.4; SAS Institute, Cary, NC).

## CALCULATION OF IONIC STRENGTH

The parameters  $w$  and  $\ell_K$  of the DNA molecule depend on the ionic strength of the surrounding solution. The ionic strength is defined as

$$I_s = \frac{1}{2} \sum_i c_i z_i^2. \quad (\text{S1})$$

Here, the sum runs over all ions in the solution,  $c_i$  is the concentration of ion species  $i$ , and  $z_i$  its valence. To compute the ionic strength, we must calculate the equilibrium concentrations  $c_i$  of all ions. Since there is some confusion in the literature (discussed below) about the ionic strength of TBE buffer, we document our calculation in some detail.

We follow the method outlined in Ref. [S7, Section 12-2]. Denote by  $C[X]$  the total amount of all species of a substance  $X$ , in neutral and ionic form. At  $N \times \text{TBE}$ , the solution contains  $C[\text{T}] = N \times 0.089$  M Tris,  $C[\text{Bo}] = N \times 0.089$  M Borate,  $C[\text{E}] = N \times 0.0020$  M EDTA, and  $C[\beta] = 0.429$  M BME. The dissociation and association constants that determine the chemical equilibrium are Tris:  $\text{p}K_b = 5.94$ ; Borate:  $\text{p}K_a = 9.24$ , EDTA:  $\text{p}K_a = \{1.99, 2.67, 6.16, 10.26\}$ ; BME:  $\text{p}K_a = 9.6$ . At the resulting pH-value of approximately 8.5, most of the EDTA is triply ionised, and we can safely ignore the minute concentrations of neutral and singly ionised EDTA. We denote the molar concentration of a species by  $[X]$ , and its activity coefficient by  $\gamma_X$ . The activity coefficients are assumed to be given by the Davies equation, as stated in Ref. [S7] (the empirical prefactors of this equation differ between sources. For our ionic strength calculations, the difference between different formulations makes a difference of two percent at most). The system

of equations that must be solved is

$$\frac{[\text{TH}^+]\gamma_{\text{TH}^+}[\text{OH}^-]\gamma_{\text{OH}^-}}{[\text{T}]\gamma_{\text{T}}} = 10^{-5.94} \quad (\text{S2})$$

$$\frac{[\text{Bo}^-]\gamma_{\text{Bo}^-}[\text{H}^+]\gamma_{\text{H}^+}}{[\text{HBo}]\gamma_{\text{HBo}}} = 10^{-9.24} \quad (\text{S3})$$

$$\frac{[\text{HE}^{3-}]\gamma_{\text{HE}^{3-}}[\text{H}^+]\gamma_{\text{H}^+}}{[\text{H}_2\text{E}^{2-}]\gamma_{\text{H}_2\text{E}^{2-}}} = 10^{-6.16} \quad (\text{S4})$$

$$\frac{[\text{E}^{4-}]\gamma_{\text{E}^{4-}}[\text{H}^+]\gamma_{\text{H}^+}}{[\text{HE}^{3-}]\gamma_{\text{HE}^{3-}}} = 10^{-10.26} \quad (\text{S5})$$

$$\frac{[\beta^-]\gamma_{\beta^-}[\text{H}^+]\gamma_{\text{H}^+}}{[\text{H}\beta]\gamma_{\text{H}\beta}} = 10^{-9.6} \quad (\text{S6})$$

$$[\text{H}^+]\gamma_{\text{H}^+} + [\text{OH}^-]\gamma_{\text{OH}^-} = 10^{-14.0} \quad (\text{S7})$$

$$[\text{T}] + [\text{TH}^+] = C[\text{T}] \quad (\text{S8})$$

$$[\text{HBo}] + [\text{Bo}^-] = C[\text{Bo}] \quad (\text{S9})$$

$$[\text{H}_2\text{E}^{2-}] + [\text{HE}^{3-}] + [\text{E}^{4-}] = C[\text{E}] \quad (\text{S10})$$

$$[\text{H}\beta] + [\beta^-] = C[\beta] \quad (\text{S11})$$

$$[\text{TH}^+] + [\text{H}^+] = \quad (\text{S12})$$

$$[\text{OH}^-] + [\text{Bo}^-] + 2[\text{H}_2\text{E}^{2-}] + 3[\text{HE}^{3-}] + 4[\text{E}^{4-}] + [\beta^-]$$

Eqs. (S2)-(S6) are the equilibrium conditions from the law of mass action, Eqs. (S7)-(S11) ensure that the total concentration of a substance is conserved, and Eq. (S12) ensures charge neutrality. The activity coefficients  $\gamma_X$  depend on the ionic strength  $I_s$  according to the Davies equation [S7],

$$\log_{10} \gamma_X = -0.51 z_X^2 \left( \frac{\sqrt{I_s}}{1 + \sqrt{I_s}} - 0.3 I_s \right). \quad (\text{S13})$$

Here,  $z_X$  is the valence of species  $X$ , and  $I_s$  is measured in units of M. Finally, the ionic strength itself is given

according to Eq. S1 by

$$I_s = 1/2 \left( [\text{TH}^+] + [\text{H}^+] + [\text{OH}^-] + [\text{Bo}^-] + 4[\text{H}_2\text{E}^{2-}] + 9[\text{HE}^{3-}] + 16[\text{E}^{4-}] + [\beta^-] \right). \quad (\text{S14})$$

We solve the system of equations (S2)-(S14) iteratively. Starting from the initial guess  $\gamma_X = 1$  for all species, Eqs. (S2)-(S12) are solved with the Mathematica routine `FindInstance`. Plugging the resulting concentrations into Eqs. (S13)-(S14) yields new values for  $\gamma_X$ , which are then used in Eqs. (S2)-(S12). This process was repeated until the ionic strength converged.

We tested our calculations by comparing with Table 1 of Ref. [S8]. We reproduce the reported ionic strengths for 0% BME and 0.5% BME to within one percent.

- 
- [S1] F. Persson and J. O. Tegenfeldt, *Chemical Society Reviews* **39**, 985 (2010).
  - [S2] L. Nyberg, F. Persson, B. Åkerman, and F. Westerlund, *Nucleic Acids Research* **41**, e184 (2013).
  - [S3] W. Reisner, J. N. Pedersen, and R. H. Austin, *Rep. Prog. Phys.* **75**, 106601 (2012).
  - [S4] N. Otsu, *IEEE Transactions on Systems, Man and Cybernetics* **9**, 62 (1979).
  - [S5] P.-S. Liao, T.-S. Chen, and P.-C. Chung, *J. Inf. Sci. Eng.* **17**, 713 (2001).
  - [S6] T. Snijders and R. Bosker, *Multilevel Analysis* (Sage Publications Ltd. London, 1999).
  - [S7] D. C. Harris, *Quantitative chemical analysis* (W.H. Freeman and Co, New York, 2010), 8th ed.
  - [S8] C.-C. Hsieh, A. Balducci, and P. S. Doyle, *Nano Letters* **8**, 1683 (2008).